Research Article

EXPERIMENTAL AND THEORETICAL PERSPECTIVES ON L-TRYPTOPHAN–FUMARIC ACID MONOHYDRATE SINGLE CRYSTALS- AN ORGANIC NONLINEAR OPTICAL SINGLE CRYSTAL FOR OPTOELECTRONIC DEVICE APPLICATIONS

Biju Joy

Department of Chemistry, St. Xavier's College, Thumba, Trivandrum, India.

ABSTRACT
A single crystal of L-tryptophan–fumaric acid monohydrate (TFAW) was grown by slow evaporation solution growth technique at room temperature. The lattice parameter of the compound was confirmed by using X-Ray diffraction analysis. Vibrational modes of the functional groups were identified by using FTIR technique. Optical transmittance spectrum was recorded by using UV-Vis-NIR spectrum. Photoconductivity measurements were also carried for the grown crystal. The second harmonic generation efficiency of the grown crystal was found to be 4 times greater than that of standard KDP. Photoluminescence study was also taken for the grown crystal. Further, HOMO-LUMO, natural bonding analysis (NBO), molecular electrostatic potential and first hyper polarizability studies were also done for the grown crystal.

Keywords: Optical materials, Crystal growth, SHG and Electrical studies.

1. INTRODUCTION

Tryptophan is natural occurring aromatic amino acids which is one of the essential amino acids for humans particularly. For many organisms, tryptophan is unavoidable to prevent illness and death. But it cannot be synthesized by the organism and be obtained from the diet. Amino acids, including tryptophan, play an important role as building blocks in biosynthesis of proteins. Tryptophan is also a biochemical precursor to the neurotransmitters melatonin and serotonin[1]. L-tryptophan is zwitterionic, as are most amino acids in the solid state, and fumaric acid is neutral. The bond lengths and angles in *L*-trypophan and fumaric acid are similar to those reported previously[2-4]. Pharmacologically, Tryptophan is among the most important classes of organic compounds. Tryptophan shows near UV absorption and emission properties, which are extensively utilized in solution phase investigations. These properties enables opportunity to avail Tryptophan in the field of optical technology[5].

Nonlinear optical crystals have been a great deal of interest in recent years due to their potential use in the fields like laser technology, optical communication, optical data storage optical signal processing[6,7]. It is also contributing number of applications in the domain of optoelectronics and photonic technologies[8]. This induces the physicists, chemists, material scientists and crystal engineers to identify a new class of NLO materials which should full fill the needs of the above fields. The search for finding the new and better NLO materials having high transparent window in visible region, high optical damage threshold and good optical frequency conversion efficiency have been engaged by several scientists. In this context, variety of organic and inorganic NLO materials has been proposed. Normally organic chromophores exhibit high and fast nonlinearities than their inorganic counterparts. This is because of their tendency to induce delocalization of π electron in their organic chromophores but in most of the inorganic materials the lacking of π electron delocalization makes them to possess only moderate optical nonlinearities. The major difficulty in inorganic materials is how to impart

the acentric packing with large second order nonlinearity value. Alternatively, the structural flexibility of the organic chromophores permits to easily modify the chemical composition in a precised manner to induce acentric packing which results in large hyperpolarizability and remarkable second order NLO activity[9,10]. The crystals which are composed of aromatic molecules with π electron donor and acceptor substitutions normally exhibit intermolecular charge transfer and leads to the required property of noncentrosymmetry and makes them good frequency conversion material .

Previously L-tryptophan–fumaric acid monohydrate crystal structure was reported by Caroline et al.,[11]. In conjunction with our ongoing work on non-linear optical organic crystals, we have directed our interest to L-tryptophan–fumaric acid monohydrateand we successfully obtained good quality single crystals of TFAW, and we report herein on its bulk growth and characterization.

2. Experimental
2.1 Synthesis and growth
Analytical grade L-tryptophan and fumaric acid were purchased from Sigma Aldrich and were used without any further purification. The slow evaporation solution growth method was used to grow single crystals of the title compound using water as a solvent at room temperature. The title compound was prepared by adding one mole of L-tryptophan and one mole of fumaric acid to water solvent. The two solutions were mixed together and stirred well using a mechanical stirrer at ambient temperature for about 5 hours to obtain a homogeneous solution. The resulting solution was filtered through Whatmann 41 filter paper. In order to prevent rapid evaporation of the solvent, the beaker containing the filtrate was covered with a thin polythene sheet. Care was taken to minimize the temperature gradient and mechanical shaking. The crystals of the title compound were harvested by the slow evaporation technique and depicted in Fig. 1.

2.2 Characterization techniques
The as grown single crystals of TFAW were subjected to single crystal XRD using an Oxford-Diffraction Xcalibur with a sapphire CCD detector and enhance diffractometer (MoKα radiation, graphite monochromator; λ=0.71073A). The optical transmittance and absorption spectra of the grown TFAW crystals with 1.502 mm thickness were recorded at room temperature using a Perkin-Elmer Lambda 35 spectrophotometer in the wavelength region of 200 to 800 nm. In the present work, the functional groups of TFAW were identified using a JASCO-FT-IR 5300

infrared spectrometer in the frequency region of 400 to 4000 cm1 by employing the KBr pellet technique with a spectral resolution of 4.0 cm-1. Photoconductivity measurements for the grown TFAW crystals were taken using a Keithley electrometer (Model 6517B). Microhardness studies for the grown TFAW crystals were carried out using a LEITZ WETZLAR Vickers microhardness pyramidal indenter attached to an incident light microscope. A Q-switched Nd:YAG laser with a fundamental wavelength of 1064 nm was used to study both the laser damage threshold and the powder SHG efficiency. The entire quantum chemical computations on LTFW were performed by using Gaussian 09 program package [12]. Geometry optimization of LTFW is performed using the Becke, three-parameter, Lee-Yang-Parr (B3LYP) functional, addition with standard 6-311++G(d,p) basis set. The NBO calculations were performed using same basis set to study the second order interactions between filled orbitals of one subsystem and vacant orbitals of another subsystems. The GaussView 5.0 visualization program was used to shape the molecular structure, MEP, HOMO and LUMO orbitals[13].

3. RESULT AND DISCUSSION
3.1 X-ray diffraction studies
The obtained unit cell parameters are a=13.624 Å, b=4.026 Å c=12.706 Å, β=114.93[0] and V=634 Å[3]. From the single crystal XRD, it is concluded that grown TFAW crystal belongs to the monoclinic crystal system with the noncentro symmetric space group of *Pc*. The lattice parameters obtained in the present study are in good agreement with the earlier reported work[11].

3.2 UV Absorption and transmittance Spectrum
UV-visible spectrum gives limited information about the structure of the molecule because the absorption of UV and visible light involves the promotion of the electron from the ground state to higher energy states. The electronic absorption spectrum of the TFAW crystal is depicted in figure 2. The spectrum reveals strong absorption bands attributed to the charge transfer transition in addition to the usual $\pi \rightarrow \pi^*$ bands of dinitrobenzene in the complex and appears between 290 and 370 nm. The longer wavelength absorption band arising due to the promotion of an electron from the highest occupied molecular orbital (donor) to the lowest unoccupied molecular orbital (acceptor) confirms the formation of charge transfer molecular complex. There is no significant absorption in the range 370- 800

nm, which provides the wide transparency window for the grown crystals.

The transmission spectrum plays a vital role in identifying the potential of a NLO material. A given NLO material can be of utility only if it has a wide transparency window without any absorption at the fundamental and second harmonic wavelengths. The spectrum is shown in figure 3. The grown crystal has no absorption beyond the wavelength 380 nm (visible region). Hence this illustrates to know the suitability of the crystal for second harmonic generation and various optical applications[14, 15]. The dependence of optical absorption coefficient with the photon energy helps to study the band structure and type of transition of electrons[15].

3.3 FTIR Analysis
The vibrations of various functional groups present in the molecule are analyzed through absorption peaks. The FTIR spectrum is shown in figure 4. The NH stretching vibrational frequency in amine functional group is absorbed at 3308 cm^{-1}. The peaks at 3028 and 2934 cm^{-1} are assigned for the OH stretching mode. The CH asymmetric and symmetric stretching mode vibrations are obtained at 2694 cm^{-1} and 2580 cm^{-1} respectively. The peaks at 1694 cm^{-1} is assigned for the NH_2 scissoring vibrational mode. The NH bending vibrational mode is revealed through the peak at 1640 cm^{-1}. The CC (in ring) stretching vibrational frequency is absorbed at 1575 cm^{-1}. In addition, the peaks at 1425 and 1410 cm^{-1} are attributed to C-O-H in-plane bending vibration. The peak at 1343 cm^{-1} is assigned for the CH rocking mode vibration. The CH wagging vibrational mode is revealed through the peak at 1295 cm^{-1}. The CN stretching vibration is absorbed at 1199 cm^{-1}. The peak at 949 cm^{-1} is assigned to the vibration of OH bending mode. The peak at 833 cm^{-1} is attributed to COO scissoring vibration. The NH wagging vibrational mode is revealed through the peak at 775 cm^{-1}. The CH deformation vibrational mode is absorbed at 649 cm^{-1}. Thus the structure of the molecule is confirmed by the presence of various functional groups.

3.4 Photoconductivity
The TFAW crystal was subjected to photoconductivity study to evaluate the crystal to be useful in the detector applications[17]. The KEITHLEY picoammeter was used to measure the photoconductivity of the crystal. The silver paste was applied on the opposite end faces of the polished crystal and it was connected into the KEITHLEY picoammeter. The dark current was recorded in absence of any radiation to the crystal at room temperature. The photo current was recorded by illuminating the crystal with 100 W halogen lamp. The photo current and dark current were measured by varying the applied field and shown in figure 5. From the figure, it implies that the crystal shows the positive response of photo current and dark current with the applied electric field. The photo current is found to be more than that of the dark current for all applied fields indicating the positive photo conducting nature of the material. The positive photoconductivity is due to the absorption and excitation of charge carries in the presence of radiation.

3.5 Mechanical studies
Mechanical properties of the grown crystal were studied using a Vickers micro-hardness tester with a Vickers diamond pyramidal indenter attached to an incident light microscope. The static indentations were made at room temperature with a constant indentation time 10 s for all indentations. The indentation marks were made on the surfaces by varying the load from 10 to 100 g. The Vickers microhardness number Hv of the crystal is calculated using the relation

$$H_V = \frac{1.8544P}{d^2} \quad kg/\mu m^2 \qquad (1)$$

Where P is the applied load in kg and d corresponds to average diagonal length in micrometre. Figure 6 shows the plot between load (P) and H_V of TFAW single crystal. From the graph, it is very clear that H_V increases with the increase of load which indicates the reverse indentation size effect (ISE). The increase in H_V with increasing load can be attributed to the electrostatic attraction between the zwitterions present in the molecule. The Meyer's index number was calculated from Meyer's law, which relates the load and indentation diagonal length and is given by

$$P = kd^n \qquad (2)$$
$$\log P = \log k + n \log d \qquad (3)$$

where k is the material constant and n is Meyer's index. The value of 'n' can be calculated using the formula $H_v = bP^{(n-2)/n}$ where b is constant. Figure 7 shows the plot between log P and log d. The slope of this straight line plot gives the value of n and is calculated as 4.38. H_V should increase with increase of P if n>2 (reverse ISE) and decrease if n<2 (normal ISE). When n=2, the hardness is independent of the load applied

and is given by Kick's law[18]. Then value agrees well with the experiment. According to Onitsch[19] and Hanneman[20] n should lie between 1 and 1.6 for harder materials and for softer materials n should be above 1.6. Thus TFAW belongs to the soft material category (n = 2.83). The stiffness constant (C11) gives details about the nature of bonding between the neighbouring atoms. C11 is the property of the material by virtue of which it can absorb maximum energy before fracture occurs. The stiffness constant (C11) is calculated from Wooster's empirical relation[21] given by C11 = $Hv^{7/4}$. The variation of stiffness constant (C11) with various loads is shown in Figure 8.

From the hardness values, the yield strength (σ_y) can be calculated. The yield strength is defined as the stress at which the material begins to deform plastically. The value of the yield strength depends on Meyer's index numbern.For n>2, σ_y can be calculated using the expression

$$\sigma_v = \frac{3-n}{2.9}\left(\frac{12.5(n-2)}{3-n}\right)^{n-2} H_v \quad (4)$$

For n<2, the yield strength is calculated using the relation

$$\sigma_v = \frac{H_v}{3} \quad\quad (5)$$

It is seen from Figure 9 that the yield strength also increases as load increases.

3.6 Powder SHG studies
The powder SHG efficiency of the powdered TFAW material was tested using the modified Kurtz and Perry technique[22]. A Q switched mode locked Nd:YAG laser beam with a wavelength of 1064 nm was used as an optical source for the SHG measurements. An input power of 4 mJ per pulse, a pulse width of 8 ns and a repetition rate of 10 Hz were used. The grown crystal was ground into uniformly sized particles of 125 to 150 mm and packed in a microcapillary tube. The same particle size of microcrystalline KDP was used as a reference for SHG measurements. The SHG behaviour of title crystal was confirmed from the emission of green radiation (532 nm). The green intensity was measured using a photomultiplier tube, transformed into electrical signals, and displayed on a storage oscilloscope. The powder second harmonic generation efficiency of TFAW is compared with that of KDP. It can be concluded that the SHG efficiency of TFAW (44 mV) is four times higher than that of the reference KDP (11 mV).

3.7 Optimized parameters
The optimized structural parameters of LTFW with atom numbering scheme are shown in figure 10 and the optimized structural parameters are calculated using the B3LYP/6-311++G(d,p) basis set and experimental data of LTFW are listed in table 1. In the LTFW compound contains L-tryptophan is a zwitterions, with a fumaric acid molecule and a water molecule are linked by N-H…O and O-H…O interactions. The bond length of N_1-H_2, N_3-H_4, N_3-H_5 and O_{40}-H_{41} are calculated to be 1.019 Å, 1.089 Å, 1.034 Å and 0.998 Å respectively. The N-H and O-H bond lengths are increasing due to formation of intra molecular hydrogen bonding of N1-H2…O3, N3-H_4…O_{40}, N3-H_5…O_{28} and O_{40}-H_{41}…O_8. The H_2-O_{33}, H_4-O_{40}, H_5-O_{28} and H_{41}-O_8 calculated distance are 1.978 Å, 1.506 Å, 1.871 Å and 1.695 Å respectively, which is extensively less than that of van dar wall's radii, which indicate the possibility of N-H…O and O-H…O intramolecular hydrogen bonding. In order to reduce steric repulsion the bond angle C_{12}-C_{15}-C_{16} (126.71°), C_{12}-C_{15}-C_{27} (127.17°) and C_{15}-C_{27}-C_{25} (132.84°) have been expended. In fumaric acid anion the carboxylic group bond angle of O_{28}-C_{34}-O_{29} is 123.09° and O_{31}-O_{39}-O_{33} is 123.09°. The DFT calculations predicted the dihedral angles of LTFW are C_{18}-N_1-C_{16}-H_{17} (178.28°), C_{16}-N_1-C_{18}-C_{19} (-178.19°), H_5-N_3-C_{10}-C_9 (-178.84°), C_{27}-C_{15}-C_{16}-H_{17}(-178.33°), C_{27}-C_{18}-C_{19}-C_{20} (-179.48°), N_1-C_{18}-C_{27}-C_{25} (-179.17°), C_{19}-C_{18}-C_{27}-C_{15} (178.97°), C_{18}-C_{19}-C_{21}-H_{22} (-179.89°), H_{20}-C_{19}-C_{21}-C_{23} (179.27°), C_{19}-C_{21}-C_{23}-H_{24} (-179.68°), H_{22}-C_{21}-C_{23}-C_{25} (-179.66°), C_{21}-C_{23}-C_{25}-H_{26} (179.08°), H_{24}-C_{23}-C_{25}-C_{27} (179.47°), C_{23}-C_{25}-C_{27}-C_{15} (-178.26°) and H_{26}-C_{25}-C_{27}-C_{18} (-179.30°) are essentially planar.

3.8 NBO analysis
NBO analysis provided an efficient method for investigating the inter and intra-molecular interactions, hybridization, delocalization of electron density within the molecule and charge transfer or conjugative interaction in a molecular system. The NBO analysis, the natural orbital interactions were analysed by using NBO 3.1 program[23] as implemented in the Gaussian'09 package at B3LYP/6-311++G(d,p) level of theory and the donor-acceptor interactions are listed in table 2. The presence of the intramolecular hydrogen bonds N-H…O and O-H…O are confirmed from the hyperconjugative interaction of $n_1O_{33}{\to}\sigma^*(N_1$-$H_2)$ and $n_2O_8{\to}\sigma^*(O_{40}$-$H_{41})$ with stabilisation energy of 15.66 kJ/mol and 25.16 kJ/mol respectively. The most dominant (n→π*) hyperconjucative interaction of $n_2O_{31}{\to}\pi^*(O_{33}$-$C_{39})$ and $n_2O_{29}{\to}\pi^*(O_{28}$-$C_{34})$

have high stabilization energies 108.27 kJ/mol and 106.34 kJ/mol respectively, which evident the intensive interaction between the n_2O and $\pi^*(O-C)$ antibonding orbital. It also manifests the electron density of orbitals $\pi^*(O_{33}-C_{39})$ and $\pi^*(O_{28}-C_{34})$ are up to 0.140 e and 0.141 e respectively. The orbital interaction of $n_1N_1 \rightarrow \pi^*(C_{15}-C_{16})$ and $n_1N_1 \rightarrow \pi^*(C_{18}-C_{19})$ have stabilization energies of 89.18 and 68.83 kJ/mol with electron density up to 0.179 e and 0.210 e in the respective antibonding orbitals. The intramolecular charge transfer interaction $\pi \rightarrow \pi^*$ are responsible for the conjugation of respective π bonds in the title compound and increase the antibonding orbital electron density. The interaction of $\pi(C_{21}-C_{23}) \rightarrow \pi^*(C_{18}-C_{19})$, $\pi(C_{21}-C_{23}) \rightarrow \pi^*(C_{25}-C_{27})$, $\pi(C_{25}-C_{27}) \rightarrow \pi^*(C_{18}-C_{19})$, $\pi(C_{25}-C_{27}) \rightarrow \pi^*(C_{21}-C_{23})$ and $\pi(C_{35}-C_{37}) \rightarrow \pi^*(O_{28}-C_{34})$ with stabilization energies of 42.08 kJ/mol, 38.81 kJ/mol, 40.70 kJ/mol, 44.21 kJ/mol and 44.21 kJ/mol respectively, and the respective antibonding orbitals electron occupancy of 0.210 e, 0.219 e, 0.210 e, 0.179 e and 0.140 e. The hyperconjugative interaction between energies of $n_2O_8 \rightarrow \sigma^*(O_7-C_9)$ and $n_2O_{28} \rightarrow \sigma^*(O_{29}-C_{34})$ are 42.37 kJ/mol and 62.05 kJ/mol respectively. These interaction energies are due to the ICT which leads to stabilize the molecule.

3.9 Frontier Molecular Orbital analysis
The frontier molecular orbital analysis explains the electronic and optical properties, UV-Vis spectra and chemical reactivity of the compound. The distributions of highest occupied molecular orbital (HOMO) and lowest unoccupied molecular orbital (LUMO) are used to analyze the electron transfer mechanism through the molecule. The HOMO-LUMO energy gap of LTFW are calculated at the gas phase using DFT/B3LYP/6-311++G(d,p) level of theory. The HOMO and LUMO energies are -9.295 eV and -6.611 eV respectively. The HOMO-LUMO energy gap of the LTFW molecule is calculated 2.684 eV, which reveals the chemical activity. The HOMO and LUMO plots are shown in figure 11. The HOMO is localized on the L-tryptophan and also LUMO is localized on the entire fumaric acid molecule. In LTFW molecule L-tryptophan act as electrophilic centre and the fumaric acid act as nucleophilic centre. According to the Koopmann's theorem [68], the ionization energy ($I = -E_{HOMO}$) and electron affinity ($A = -E_{LUMO}$) of the LTFW molecule are 9.295 eV and 6.611 eV respectively. The

electronegativity (χ), chemical reactivity (μ), softness (s) and other calculated reactivity descriptors are listed in table 3. The HOMO-LUMO energy gap is small, it promotes the interaction between HOMO of electron donors and LUMO of electron acceptors and also stabilize the molecule and thereby NLO activity.

3.10 Molecular Electrostatic Potential
The molecular electrostatic potential is widely used as reactivity towards electrophilic and nucleophilic attacks as well as hydrogen bonding interactions. The MEP surface for LTFW was generated by mapping B3LYP/6-311++G(d,p) method, electrostatic potential onto the molecular electron density surface is shown in figure 12 the dissimilar values of electrostatic potential at the surface are indicated by different colors. In MEP of LTFW, the isosurface=-0.211 a.u. representing the regions that eagerly donate electron (nucleophilic centre) and isosurface= +0.211 a.u. representing the regions that accept electrons (electrophilic centre). In MEP surface the maximum positive region, which is preferred site for nucleophilic attack is depicted as blue, while the maximum negative region is selected site for electrophilic attack is represented as red. As seen from figure 12, the red region electrophilic reactivity was essentially localized on the oxygen atoms, whereas the blue region nucleophilic reactivity of the molecule was mainly localized on the carboxylic group hydrogen and nitrogen.

3.11 Hyperpolarizability
The interactions of electromagnetic fields in various materials produce the nonlinear optical (NLO) effects by altering the phase, frequency, amplitude or other propagation characteristics from the incident fields. To design the novel NLO materials, the theoretical investigation plays a key role in understanding the structure–property relationship. As the basis becomes larger, one expects a better description of the compound and accordingly more accurate results. In the view of these points, B3LYP/6-311G++(d,p) method has been used for the present study. The complete equations for calculating the magnitude of the total static dipole moment (μ), mean polarizability (α), anisotropy of polarizability ($\Delta\alpha$) and first order hyperpolarizability (β) from Gaussian output are given below

$$\mu = \sqrt{\left(\mu_x^2 + \mu_x^2 + \mu_x^2\right)} \qquad (6)$$

$$\alpha = \frac{(\alpha_{xx} + \alpha_{yy} + \alpha_{zz})}{3} \qquad (7)$$

$$\Delta\alpha = \sqrt{2}\left[(\alpha_{xx} - \alpha_{yy})^2 + (\alpha_{yy} - \alpha_{zz})^2 + (\alpha_{zz} - \alpha_{xx})^2 + 6\alpha_{xx}^2\right]^{1/2} \qquad (8)$$

$$\beta = \left[(\beta_{xxx} + \beta_{xyy} + \beta_{xzz})^2 + (\beta_{yyy} + \beta_{yzz} + \beta_{yxx})^2 + (\beta_{zzz} + \beta_{zxx} + \beta_{zyy})^2\right]^{1/2} \qquad (9)$$

The polarizabilities and hyperpolarizability are reported in terms of atomic units (a.u) and the calculated values have been converted by using 1 a.u. = 0.1482×10^{-24} esu for α and 1 a.u. = 8.6393×10^{-33} cm5/esu for β. In the calculations, the values of the calculated dipole moment (μ), mean polarizability (α) and anisotropy of polarizability ($\Delta\alpha$) are 3.576697 Debye, 40.048 Å esu, 35.172Å esu. The calculated first hyperpolarizability value (β) which is an important key factors for NLO properties of molecular system is equal to 804.51×10^{-31} cm^5 esu^{-1}. In NLO studies, the urea is used as reference and its calculated values of μ, α, $\Delta\alpha$ and β are found to be 4.303 Debye, 0.139 Å esu, 0.934 Å esu, 0.563×10^{-31} cm^5 esu^{-1}respectively. In comparison with urea, the hyperpolarizability value of TFAW is more than 30.33 times that of urea (Table 4). A large first hyperpolarizability value is a requirement of a good NLO material. The results indicate that the studied compound is a good NLO material due to its high β values. The largest value is noted to be in the β_{yyy} direction; this may be because the subsequent delocalization of the electron cloud occurs more in this particular direction.

4. CONCLUSION

Nonlinear optical single crystals of TFAW were synthesized and grown by adopting a slow evaporation method at room temperature. UV-Vis analysis reveals a lower cutoff wavelength at 370 nm and exhibits the absence of absorption in the visible region. The TFAW crystal showed transparency beyond the 370 nm wavelength (visible) region, which is a desirable property for various NLO applications. The presence of various functional groups in crystal was analyzed by The FTIR spectrum. The positive photoconducting nature of the crystals conveys their suitability for optical applications. The Vickers microhardness test revealed the reverse indentation nature of the material. The SHG efficiency of the TFAW crystal was four times that of KDP. This demonstrates the suitability of the crystal for second harmonic generation applications. Molecular electrostatic potential analysis was performed using the optimized geometry of the molecule and provided vital details on the nucleophilic and electrophilic sites of 2A5C4C. The frontier molecular orbital analysis provided detailed information about the chemical stability, hardness and charge distribution of TFAW. NBO analysis revealed inter- and intramolecular interactions in the TFAW. The predicted first hyperpolarizability was found to be 30.33 times greater than that of urea. All above studies suggest that TFAW could be a potential candidate for optoelectronics applications.

Fig. 1: As grown crystals of TFAW
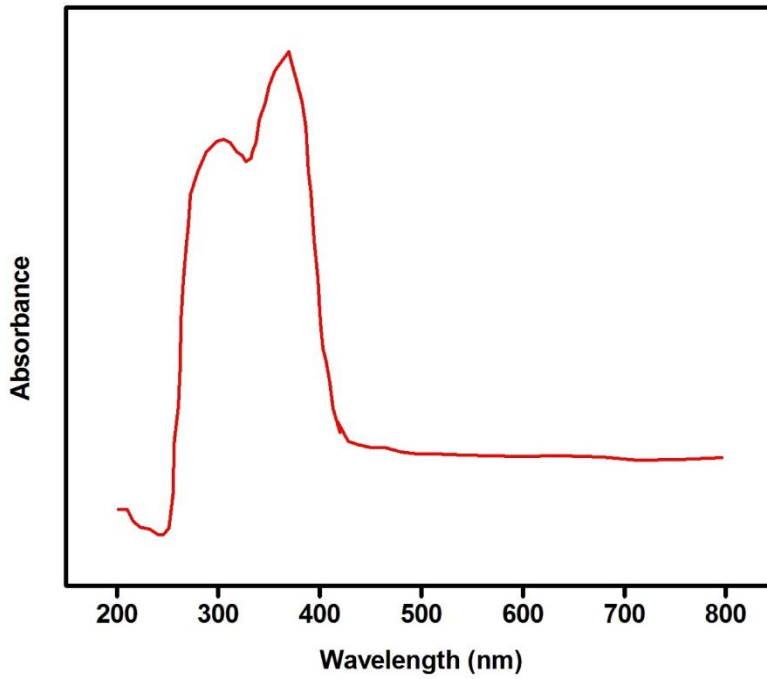
Fig. 2: Optical absorption spectrum of TFAW
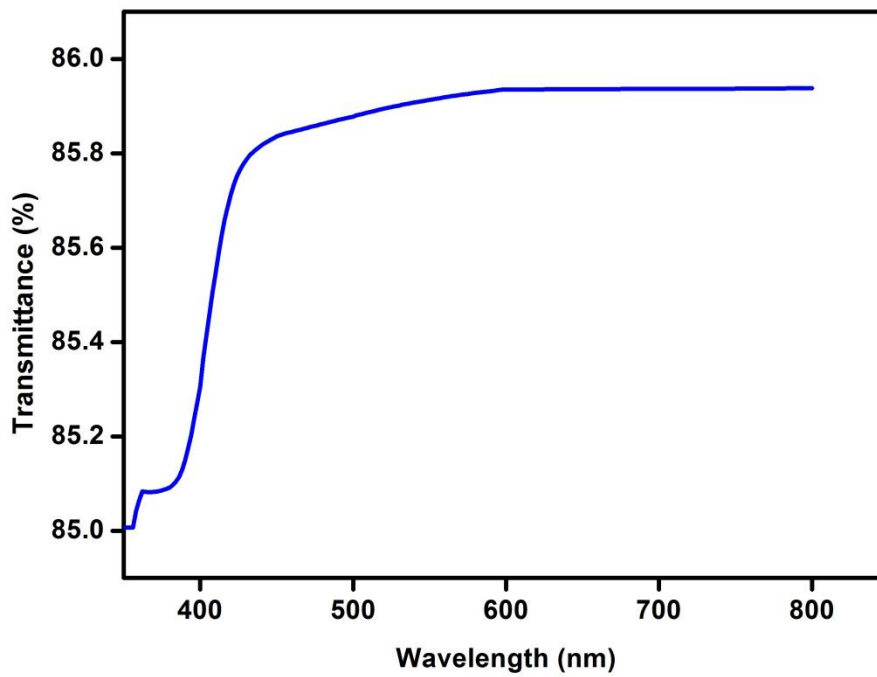
Fig. 3: Optical transmittance spectrum of TFAW
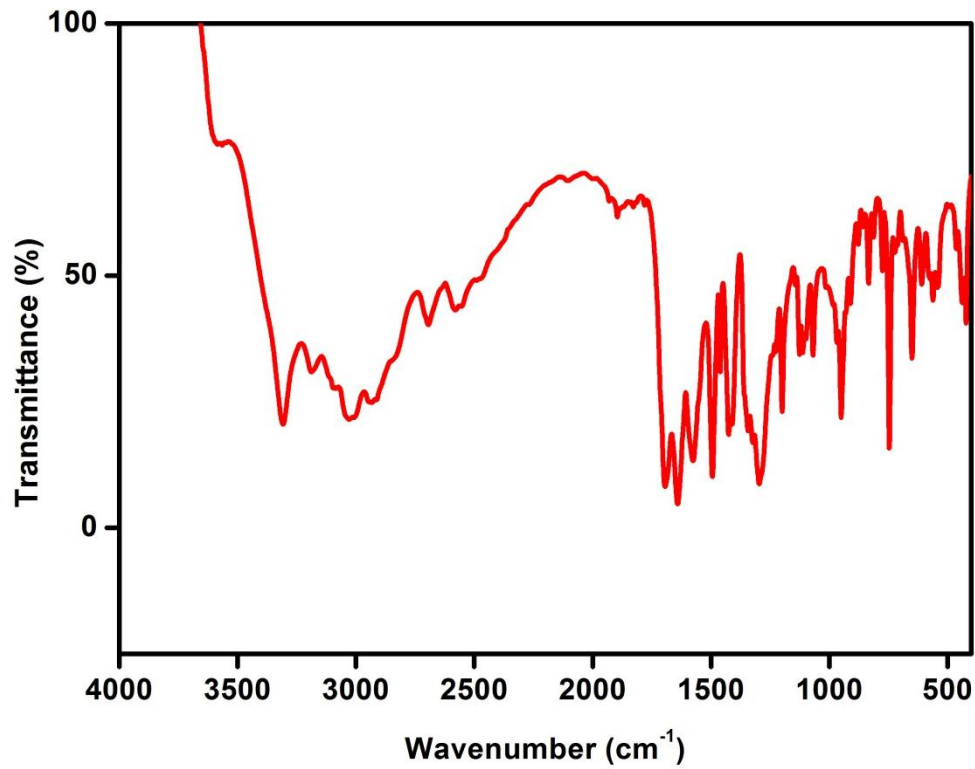
Fig. 4: FTIR spectrum of TFAW
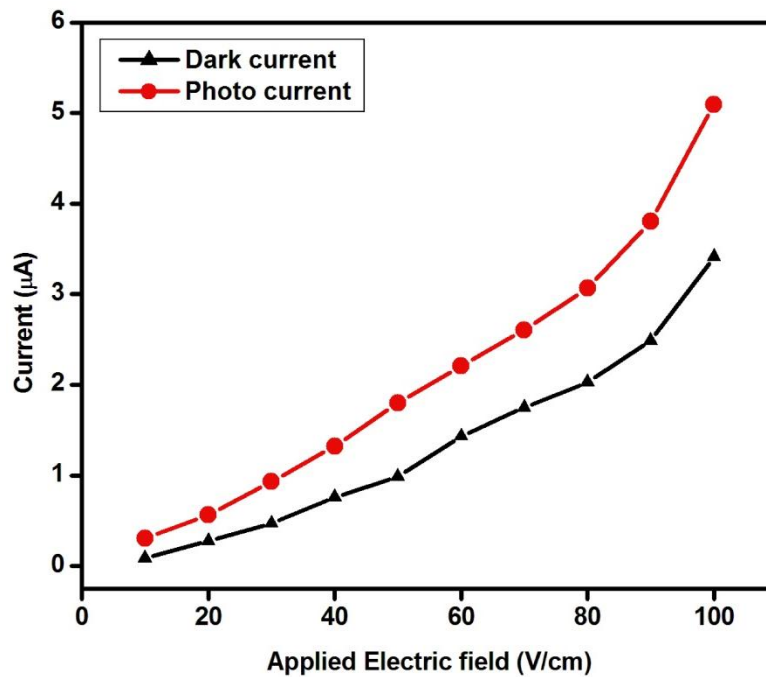
Fig. 5: Photoconductivity response of TFAW
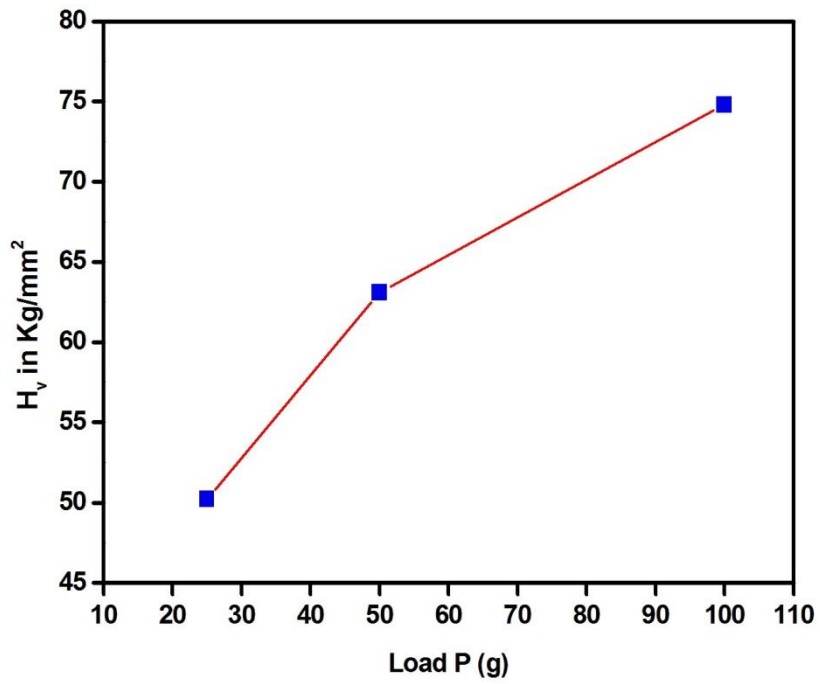
Fig. 6: H_v Vs load P
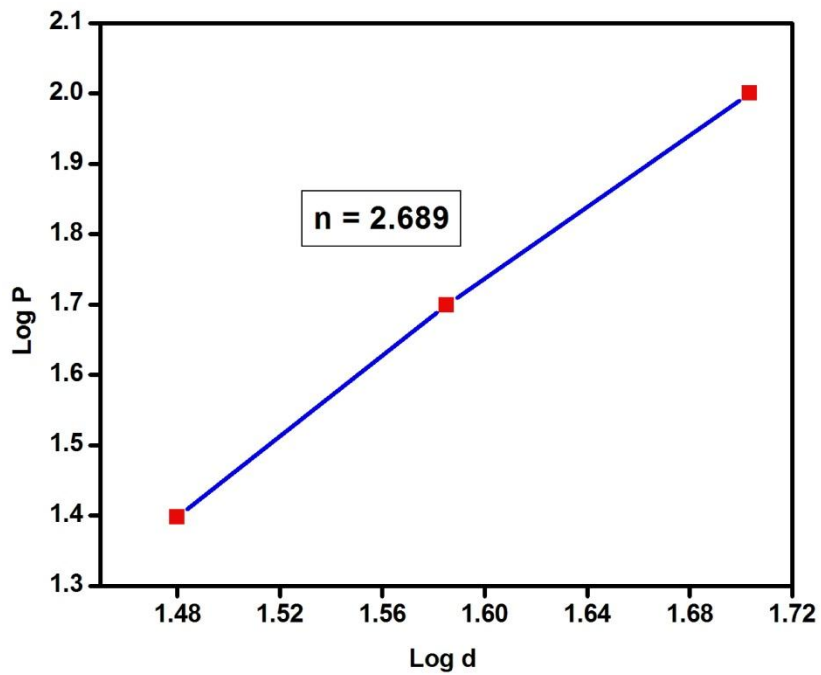
Fig. 7: Log P Vs Log d
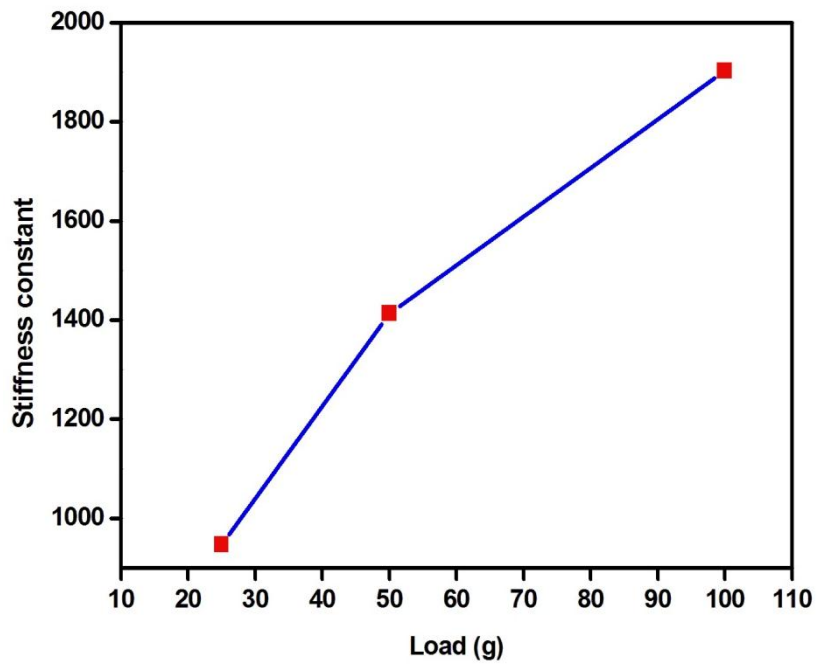
Fig. 8: Stiffness cnstant Vs Load
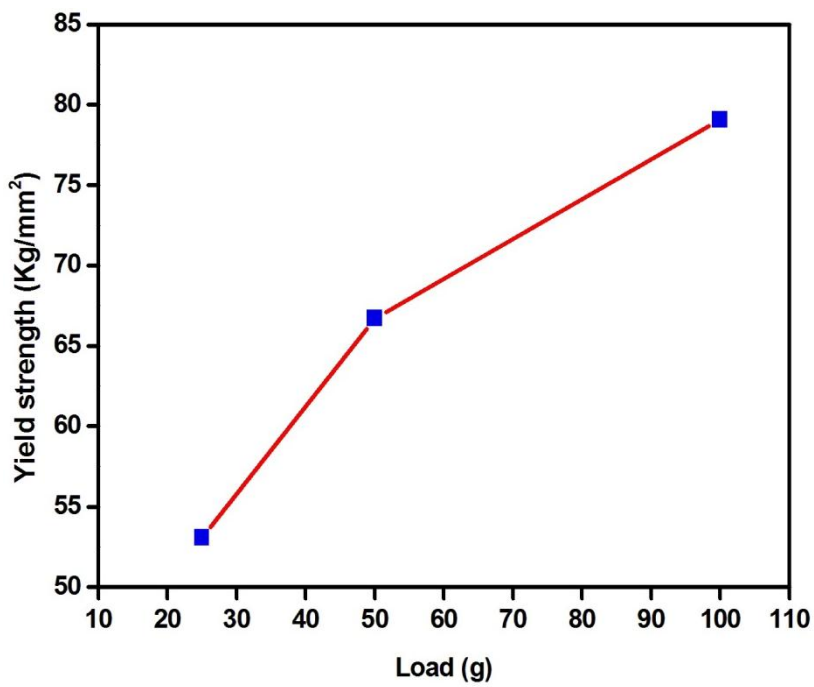
Fig. 9: Yield strength Vs Load
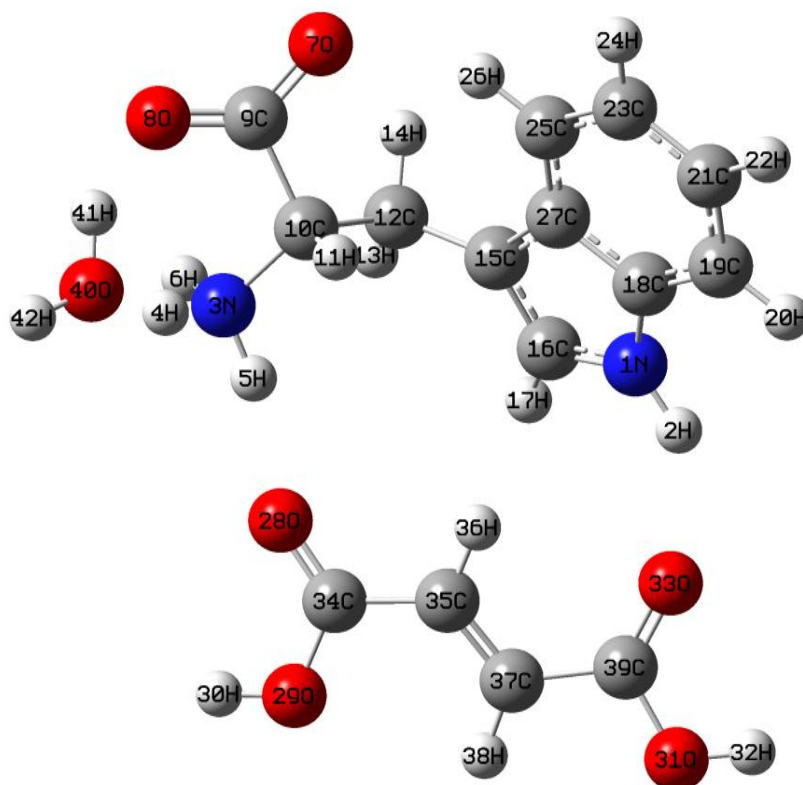
**Fig. 10: Optimized molecular structure of LTFW calculated
at B3LYP/6-311++G(d,p) level of theory**

E_{HOMO} = -9.295 eV

Eg= 2.684 eV

E_{LUMO} = -6.611 eV
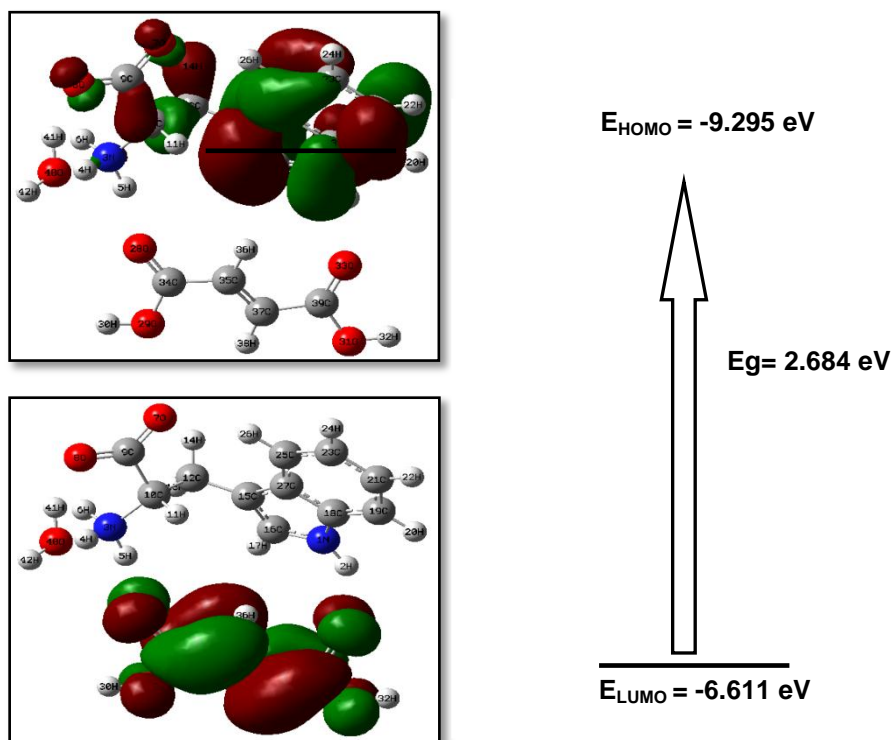
**Fig.11: Frontier molecular orbitals and energies
for the HOMO and LUMO of LTFW**
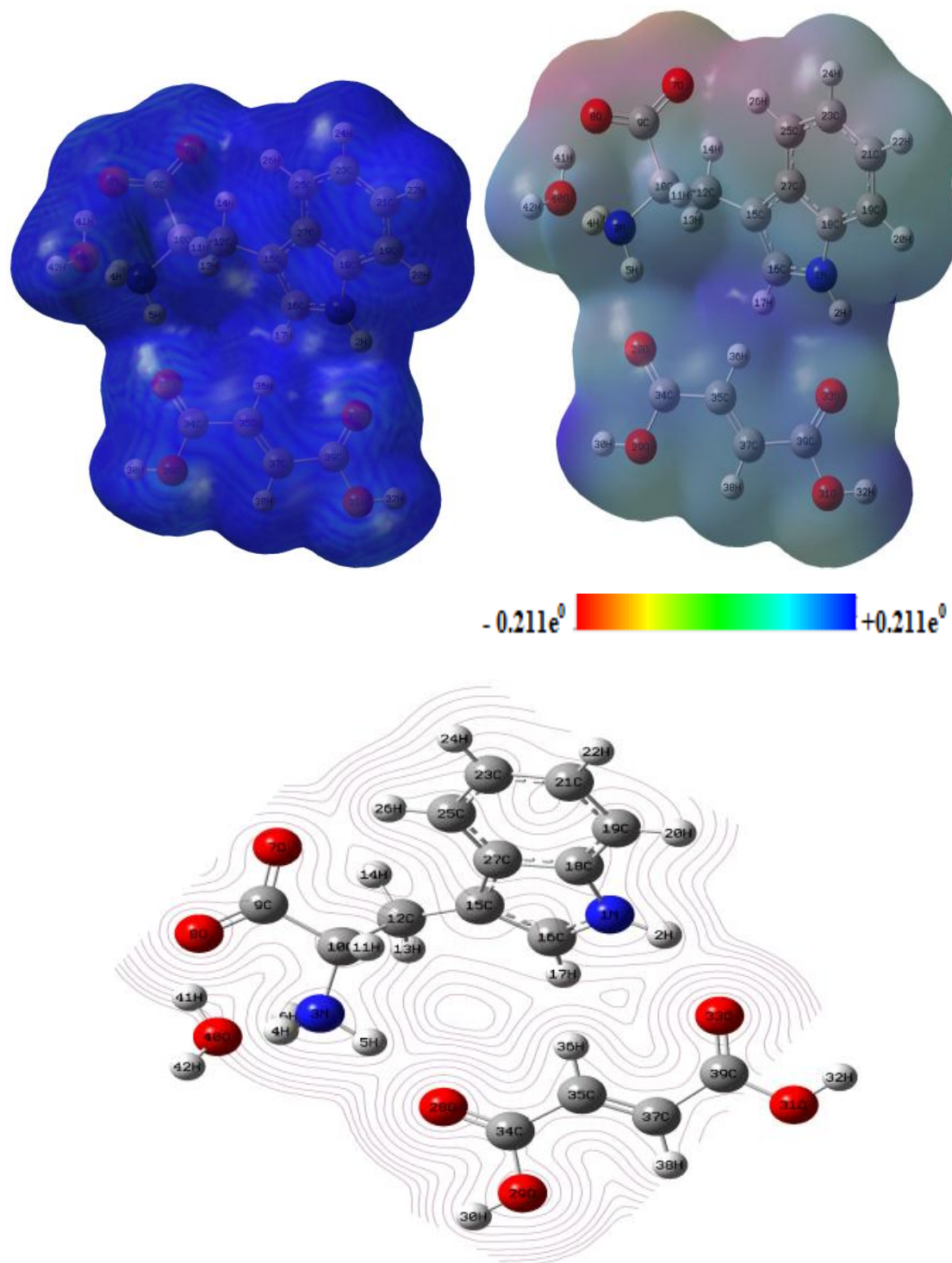
Fig. 12: Total electron density (TED), molecular electrostatic potential (MSEP) and electrostatic potential contour map of LTFW

Table 1: Optimized geometric parameters of LTFW by using B3LYP/6-311++G(d,p)

Bond lengths	B3LYP (Å)	XRD (Å)	Bond angles	B3LYP (°)	XRD (°)	Dihedral Angles	B3LYP (°)	XRD (°)
N_1-H_2	1.019	0.850	H_2-N_1-C_{16}	122.80	123.56	H_2-N_1-C_{16}-C_{15}	171.34	-179.24
N_1-C_{16}	1.356	1.359	H_2-N_1-C_{18}	127.13	127.64	H_2-N_1-C_{16}-H_{17}	-9.19	0.78
N_1-C_{18}	1.409	1.370	C_{16}-N_1-C_{18}	109.59	108.79	C_{18}-N_1-C_{16}-C_{15}	-1.19	0.13
H_2-O33	1.978	2.110	N_1-H_2-O_{33}	143.65	158.00	C_{18}-N_1-C_{16}-H_{17}	178.28	-179.85
N_3-H_4	1.089	0.964	H_4-N_3-H_5	108.07	108.14	H_2-N_1-C_{18}-C_{19}	9.69	1.48
N_3-H_5	1.034	0.939	H_4-N_3-H_6	106.47	105.12	H_2-N_1-C_{18}-C_{27}	-171.32	179.86
N_3-H_6	1.024	0.918	H_4-N_3-C_{10}	109.29	112.59	C_{16}-N_1-C_{18}-C_{19}	-178.19	-177.85
N_3-C_{10}	1.516	1.482	H_5-N_3-H_6	110.03	108.18	C_{16}-N_1-C_{18}-C_{27}	0.80	0.52
H_4-O_{40}	1.506	1.870	H_5-N_3-C_{10}	112.58	109.26	H_5-N_3-O_{40}-H_{41}	171.98	162.21
H_5-O_{28}	1.871	2.280	H_6-N_3-C_{10}	110.20	113.31	H_5-N_3-O_{40}-H_{42}	-40.10	-14.69
O_7-C_9	1.269	1.240	N_3-H_5-O_{28}	167.37	174.00	H_6-N_3-O_{40}-H_{41}	-65.85	-79.33
O_8-C_9	1.273	1.285	C_9-O_8-H_{41}	125.23	120.00	H_6-N_3-O_{40}-H_{42}	82.07	103.77
O_8-H_{41}	1.695	1.970	O_7-C_9-O_8	130.45	123.93	C_{10}-N_3-O_{40}-H_{41}	48.94	41.16
C_9-C_{10}	1.590	1.521	O_7-C_9-C_{10}	113.37	116.79	C_{10}-N_3-O_{40}-H_{42}	-163.14	-135.74
C_{10}-H_{11}	1.095	0.980	O_8-C_9-C_{10}	116.15	119.22	H_4-N_3-H_5-O_{28}	23.40	-62.84
C_{10}-C_{12}	1.563	1.529	N_3-C_{10}-C_9	110.51	110.36	H_6-N_3-H_5-O_{28}	-92.47	-176.18
C_{12}-H_{13}	1.096	0.970	N_3-C_{10}-H_{11}	105.42	109.03	C_{10}-N_3-H_5-O_{28}	144.20	60.04
C_{12}-H_{14}	1.099	0.969	N_3-C_{10}-C_{12}	113.10	110.18	H_4-N_3-C_{10}-C_9	-58.74	-55.43
C_{12}-C_{15}	1.486	1.491	C_9-C_{10}-H_{11}	106.27	108.95	H_4-N_3-C_{10}-H_{11}	55.68	64.20
C_{15}-C_{16}	1.416	1.355	C_9-C_{10}-C_{12}	110.36	109.36	H_4-N_3-C_{10}-C_{12}	176.96	-176.30
C_{15}-C_{27}	1.441	1.433	H_{11}-C_{10}-C_{12}	110.86	108.93	H_5-N_3-C_{10}-C_9	-178.84	-175.60
C_{16}-H_{17}	1.078	0.930	C_{10}-C_{12}-H_{13}	110.61	108.37	H_5-N_3-C_{10}-H_{11}	-64.41	-55.97
C_{18}-C_{19}	1.386	1.390	C_{10}-C_{12}-H_{14}	105.36	108.30	H_5-N_3-C_{10}-C_{12}	56.86	63.53
C_{18}-C_{27}	1.425	1.412	C_{10}-C_{12}-C_{15}	112.09	115.71	H_6-N_3-C_{10}-C_9	57.92	63.70
C_{19}-H_{20}	1.084	0.930	H_{13}-C_{12}-H_{14}	108.36	107.48	H_6-N_3-C_{10}-H_{11}	172.35	-176.67
C_{19}-C_{21}	1.416	1.366	H_{13}-C_{12}-C_{15}	110.65	108.34	H_6-N_3-C_{10}-C_{12}	-66.37	-57.17
C_{21}-H_{22}	1.084	0.930	H_{14}-C_{12}-C_{15}	109.57	108.36	N_3-H_5-C_{34}-O_{29}	83.46	179.02
C_{21}-C_{23}	1.400	1.397	C_{12}-C_{15}-C_{16}	126.71	126.57	N_3-H_5-C_{34}-C_{35}	-98.79	-42.87
C_{23}-H_{24}	1.084	0.931	C_{12}-C_{15}-C_{27}	127.17	127.37	H_{41}-O_8-C_9-O_7	-142.65	-105.35
C_{23}-C_{25}	1.408	1.365	C_{16}-C_{15}-C_{27}	106.06	105.84	H_{41}-O_8-C_9-C_{10}	35.04	77.57
C_{25}-H_{26}	1.087	0.929	N_1-C_{16}-H_{17}	109.89	111.12	C_9-O_8-H_{41}-O_{40}	-38.72	-70.94
C_{25}-C_{27}	1.409	1.402	N_1-C_{16}-H_{17}	121.51	124.46	O_7-C_9-C_{10}-N_3	-160.97	161.61
O_{28}-C_{34}	1.247	1.218	C_{15}-C_{16}-H_{17}	128.60	124.42	O_7-C_9-C_{10}-H_{11}	85.15	41.93
O_{29}-H_{30}	0.982	0.820	N_1-C_{18}-C_{19}	130.47	131.18	O_7-C_9-C_{10}-C_{12}	-35.11	-77.03
O_{29}-C_{34}	1.357	1.303	N_1-C_{18}-C_{27}	107.03	107.14	O_8-C_9-C_{10}-N_3	20.95	-21.11
O_{31}-H_{32}	0.983	0.820	C_{19}-C_{18}-C_{27}	122.50	121.66	O_8-C_9-C_{10}-H_{11}	-92.94	-140.78
O_{31}-C_{39}	1.356	1.285	C_{18}-C_{19}-H_{20}	122.23	121.07	O_8-C_9-C_{10}-C_{12}	146.80	100.26
O_{33}-C_{39}	1.245	1.229	C_{18}-C_{19}-C_{21}	117.01	117.86	N_3-C_{10}-C_{12}-H_{13}	11.54	57.16
C_{34}-C_{35}	1.469	1.466	H_{20}-C_{19}-C_{21}	120.76	121.07	N_3-C_{10}-C_{12}-H_{14}	128.43	173.46
C_{35}-H_{36}	1.083	0.930	C_{19}-C_{21}-H_{22}	118.85	119.31	N_3-C_{10}-C_{12}-C_{15}	-112.47	-64.70
C_{35}-C_{37}	1.343	1.297	C_{19}-C_{21}-C_{23}	121.53	121.35	C_9-C_{10}-C_{12}-H_{13}	-112.84	-64.31
C_{37}-H_{38}	1.084	0.931	H_{22}-C_{21}-C_{23}	119.62	119.34	C_9-C_{10}-C_{12}-H_{14}	4.05	51.99
C_{37}-C_{39}	1.481	1.475	C_{21}-C_{23}-H_{24}	119.52	119.13	C_9-C_{10}-C_{12}-C_{15}	123.15	173.83
O_{40}-H_{41}	0.998	0.883	C_{21}-C_{23}-C_{25}	121.16	121.65	H_{11}-C_{10}-C_{12}-H_{13}	129.69	176.71
O_{40}-H_{42}	0.968	0.845	H_{24}-C_{23}-C_{25}	119.32	119.22	H_{11}-C_{10}-C_{12}-H_{14}	-113.42	-66.98
			C_{23}-C_{25}-H_{26}	121.50	120.57	H_{11}-C_{10}-C_{12}-C_{15}	5.69	54.85
			C_{23}-C_{25}-C_{27}	118.07	118.83	C_{10}-C_{12}-C_{15}-C_{16}	110.20	101.22
			H_{26}-C_{25}-C_{27}	120.43	120.60	C_{10}-C_{12}-C_{15}-C_{27}	-66.81	-84.91
			C_{15}-C_{27}-C_{18}	107.42	107.09	H_{13}-C_{12}-C_{15}-C_{16}	-13.78	-20.65
			C_{15}-C_{27}-C_{25}	132.84	134.27	H_{13}-C_{12}-C_{15}-C_{27}	169.21	153.22
			C_{18}-C_{27}-C_{25}	119.73	118.63	H_{14}-C_{12}-C_{15}-C_{16}	-133.20	-136.97
			H_{30}-O_{29}-C_{34}	112.83	109.50	H_{14}-C_{12}-C_{15}-C_{27}	49.79	36.90
			H_{32}-O_{31}-C_{39}	112.83	109.49	C_{12}-C_{15}-C_{16}-N_1	-176.43	174.22
			H_2-O_{33}-C_{39}	154.56	147.12	C_{12}-C_{15}-C_{16}-H_{17}	4.15	-5.79
			O_{28}-C_{34}-O_{29}	122.77	123.43	C_{27}-C_{15}-C_{16}-N_1	1.09	-0.71
			O_{28}-C_{34}-C_{35}	122.85	121.51	C_{27}-C_{15}-C_{16}-H_{17}	-178.33	179.27
			O_{29}-C_{34}-C_{35}	114.37	115.06	C_{12}-C_{15}-C_{27}-C_{18}	176.93	-173.87
			C_{34}-C_{35}-H_{36}	114.41	117.38	C_{12}-C_{15}-C_{27}-C_{25}	-4.18	5.08
			C_{34}-C_{35}-C_{37}	125.24	125.28	C_{16}-C_{15}-C_{27}-C_{18}	-0.58	1.01
			H_{36}-C_{35}-C_{37}	120.31	117.34	C_{16}-C_{15}-C_{27}-C_{25}	178.32	179.96
			C_{35}-C_{37}-H_{38}	122.68	119.29	N_1-C_{18}-C_{19}-H_{20}	-0.63	-0.81
			C_{35}-C_{37}-C_{39}	119.81	121.47	N_1-C_{18}-C_{19}-C_{21}	178.71	179.20
			H_{38}-C_{37}-C_{39}	117.51	119.24	C_{27}-C_{18}-C_{19}-H_{20}	-179.48	-178.98
			O_{31}-C_{39}-O_{33}	123.09	124.47	C_{27}-C_{18}-C_{19}-C_{21}	-0.14	1.03
			O_{31}-C_{39}-C_{37}	111.47	114.56	N_1-C_{18}-C_{27}-C_{15}	-0.11	-0.94
			O_{33}-C_{39}-C_{37}	125.44	120.97	N_1-C_{18}-C_{27}-C_{25}	-179.17	179.91
			H_4-O_{40}-H_{41}	95.73	128.96	C_{19}-C_{18}-C_{27}-C_{15}	178.97	177.62
			H_4-O_{40}-H_{42}	143.02	123.71	C_{19}-C_{18}-C_{27}-C_{25}	-0.09	-1.52
			H_{41}-O_{40}-H_{42}	116.33	107.31	C_{18}-C_{19}-C_{21}-H_{22}	-179.89	179.87

			O_8-H_{41}-O_{40}	141.19	-165.16	C_{18}-C_{19}-C_{21}-C_{23}	-0.08	-0.12
						H_{20}-C_{19}-C_{21}-H_{22}	-0.53	-0.12
						H_{20}-C_{19}-C_{21}-C_{23}	179.27	179.88
						C_{19}-C_{21}-C_{23}-H_{24}	-179.68	179.72
						C_{19}-C_{21}-C_{23}-C_{25}	0.54	-0.27
						H_{22}-C_{21}-C_{23}-H_{24}	0.12	-0.27
						H_{22}-C_{21}-C_{23}-C_{25}	-179.66	179.74
						C_{21}-C_{23}-C_{25}-H_{26}	179.08	179.73
						C_{21}-C_{23}-C_{25}-C_{27}	-0.75	-0.23
						H_{24}-C_{23}-C_{25}-H_{26}	-0.71	-0.26
						H_{24}-C_{23}-C_{25}-C_{27}	179.47	179.77
						C_{23}-C_{25}-C_{27}-C_{15}	-178.26	-177.76
						C_{23}-C_{25}-C_{27}-C_{18}	0.53	1.09
						H_{26}-C_{25}-C_{27}-C_{15}	1.92	2.27
						H_{26}-C_{25}-C_{27}-C_{18}	-179.30	-178.87
						H_{30}-O_{29}-C_{34}-O_{28}	-0.29	1.42
						H_{30}-O_{29}-C_{34}-C_{35}	-178.98	-178.42
						H_{32}-O_{31}-C_{39}-O_{33}	0.51	-4.65
						H_{32}-O_{31}-C_{39}-C_{37}	179.63	175.76
						H_2-O_{33}-C_{39}-O_{31}	170.97	102.55
						H_2-O_{33}-C_{39}-C_{37}	-8.04	-77.89
						O_{28}-C_{34}-C_{35}-H_{36}	9.50	-1.10
						O_{28}-C_{34}-C_{35}-C_{37}	-168.19	178.85
						O_{29}-C_{34}-C_{35}-H_{36}	-171.81	178.75
						O_{29}-C_{34}-C_{35}-C_{37}	10.51	-1.31
						C_{34}-C_{35}-C_{37}-H_{38}	-4.05	-1.91
						C_{34}-C_{35}-C_{37}-C_{39}	174.97	178.06
						H_{36}-C_{35}-C_{37}-H_{38}	178.39	178.03
						H_{36}-C_{35}-C_{37}-C_{39}	-2.59	-2.00
						C_{35}-C_{37}-C_{39}-O_{31}	171.52	-175.94
						C_{35}-C_{37}-C_{39}-O_{33}	-9.38	4.46
						H_{38}-C_{37}-C_{39}-O_{31}	-9.41	4.03
						H_{38}-C_{37}-C_{39}-O_{33}	169.69	-175.57
						H_4-O_{40}-H_{41}-O_8	-7.98	8.88
						H_{42}-O_{40}-H_{41}-O_8	-168.98	-70.19

Table 2: Second order perturbation theory analysis of Fock matrix in NBO basis including the stabilization energies using DFT at B3LYP/6-311++G(d,p) level

Donor (*i*)	ED(i) (e)	Acceptor (*j*)	ED(*j*) (e)	E(2)[a] (kJ/mol)	E(*j*)-E(*i*)[b] (a.u)	F(*i, j*)[c] (a.u)
$\pi(C_{15}\text{-}C_{16})$	0.935	$\pi^*(C_{25}\text{-}C_{27})$	0.219	36.80	0.32	0.07
$\pi(C_{18}\text{-}C_{19})$	0.828	$\pi^*(C_{21}\text{-}C_{23})$	0.179	37.72	0.30	0.07
$\pi(C_{18}\text{-}C_{19})$		$\pi^*(C_{25}\text{-}C_{27})$	0.219	35.92	0.29	0.07
$\pi(C_{21}\text{-}C_{23})$	0.812	$\pi^*(C_{18}\text{-}C_{19})$	0.210	42.08	0.27	0.07
$\pi(C_{21}\text{-}C_{23})$		$\pi^*(C_{25}\text{-}C_{27})$	0.219	38.81	0.27	0.06
$\pi(C_{25}\text{-}C_{27})$	0.810	$\pi^*(C_{15}\text{-}C_{16})$	0.179	36.38	0.23	0.06
$\pi(C_{25}\text{-}C_{27})$		$\pi^*(C_{18}\text{-}C_{19})$	0.210	40.70	0.27	0.07
$\pi(C_{25}\text{-}C_{27})$		$\pi^*(C_{21}\text{-}C_{23})$	0.179	44.21	0.28	0.07
n_1N_1	0.821	$\pi^*(C_{15}\text{-}C_{16})$	0.179	89.18	0.28	0.10
n_1N_1		$\pi^*(C_{18}\text{-}C_{19})$	0.210	68.83	0.32	0.09
n_2O_7	0.938	$\sigma^*(O_8\text{-}C_9)$	0.026	41.03	0.78	0.11
n_2O_7		$\sigma^*(C_9\text{-}C_{10})$	0.059	38.35	0.55	0.09
n_2O_8	0.933	$\sigma^*(O_7\text{-}C_9)$	0.024	42.37	0.80	0.12
n_2O_8		$\sigma^*(C_9\text{-}C_{10})$	0.059	30.52	0.57	0.08
n_1O_8	0.976	$\sigma^*(O_{40}\text{-}H_{41})$	0.027	23.99	1.08	0.10
n_2O_8	0.933	$\sigma^*(O_{40}\text{-}H_{41})$	0.027	25.16	0.69	0.08
n_1O_{28}	0.935	$\sigma^*(N_3\text{-}H_5)$	0.023	23.82	1.14	0.10
n_1O_{33}	0.931	$\sigma^*(N_1\text{-}H_2)$	0.016	15.66	1.16	0.08
$\pi(C_{35}\text{-}C_{37})$	0.921	$\pi^*(O_{28}\text{-}C_{34})$	0.140	44.21	0.27	0.07
$\pi(C_{35}\text{-}C_{37})$		$\pi^*(O_{33}\text{-}C_{39})$	0.141	39.40	0.28	0.07
n_2O_{28}	0.933	$\sigma^*(O_{29}\text{-}C_{34})$	0.044	62.05	0.63	0.12
n_2O_{28}		$\sigma^*(C_{34}\text{-}C_{35})$	0.025	26.33	0.72	0.09
n_1O_{29}	0.986	$\sigma^*(O_{28}\text{-}C_{34})$	0.012	16.96	1.13	0.09
n_2O_{29}	0.899	$\pi^*(O_{28}\text{-}C_{34})$	0.140	106.34	0.31	0.12
n_1O_{31}	0.987	$\sigma^*(O_{33}\text{-}C_{39})$	0.013	17.21	1.13	0.09
n_2O_{31}	0.892	$\pi^*(O_{33}\text{-}C_{39})$	0.141	108.27	0.31	0.12
n_2O_{33}	0.931	$\sigma^*(O_{31}\text{-}C_{39})$	0.044	61.76	0.62	0.12
n_2O_{33}		$\sigma^*(C_{37}\text{-}C_{39})$	0.028	31.53	0.69	0.09

Table 3: Calculated quantum chemical molecular orbital properties for LTFW at DFT/B3LYP/6-311++G(d,p) method

Parameters	B3LYP/C6-311++G(d,p)
HOMO energy, E_{HOMO} (eV)	-9.295
LUMO energy, E_{LUMO} (eV)	-6.611
HOMO- LUMO energy gap, ΔE_{GAP} (eV)	2.684
Ionisation potential, IP (eV)	9.295
Electron affinity, EA (eV)	6.611
Electronegativity, χ (eV)	7.953
Chemical hardness, η (eV)	1.342
Global softness, S $(eV)^{-1}$	0.373
Chemical potential, μ (eV)	-7.953
Electrophilicity index, ω (eV)	23.566
Total energy change, ΔE_T (eV)	-0.336
Overall energy balance, ΔE (eV)	-2.684

Table 4: The predicted values of first hyperpolarizability (b), mean polarizability (a), anisotropy of the polarizability (Da), and total static dipole moment of LTFW by DFT/B3LYP/cc-pVTZ method

β components	esu($\times 10^{-31}$)
β_{xxx}	-381.72
β_{xxy}	333.44
β_{xyy}	-2803.52
β_{yyy}	1572.36
β_{xxz}	-35.75
β_{xyz}	8.86
β_{yyz}	59.37
β_{xzz}	6.95
β_{yzz}	-24.67
β_{zzz}	6.35
First hyperpolarizability, β_{total}	804.51
α components	esu($\times 10^{-24}$)
α_{xx}	50.308
α_{xy}	-16.491
α_{yy}	53.126
α_{xz}	-1.3730
α_{yz}	-5.3909
α_{zz}	16.711
Mean Polarizability, α	40.048
Anisotropy of Polarizability, $\Delta\alpha$	35.172
μ components	Debye
μ_x	-3.54288
μ_y	-0.3555
μ_z	-0.33819
Total Dipole moment, μ_{total}	3.576697

REFERENCES

1. Slominski A, Semak I, Pisarchik A, Sweatman T, Szczesniewski A and Wortsman J. FEBS Lett. 2002;511(1-3):102–106.
2. Gorbitz CH. Acta Cryst. 2006;C62:328–330.
3. Gorbitz CH, Tornroos KW and Day GM. Acta Cryst. 2012;B68:549–557.
4. Goswami S, Mahapatra AK, Nigam GD, Chinnakali K, Fun HK and Razak IA. Acta Cryst. 1999;C55:583–585.
5. Demchenko AP. In Ultraviolet Spectroscopy of Proteins. Berlin, Springer. 1986.
6. Marcy HO, Rosker MJ, Warren LF, Cunningham PH, Thomas CA, DeLoach LA, Velsko SP, Ebbers CA, Liao JH and Kanatzidis MG. Opt Lett. 1995;20:252-254.
7. Chemla DS and Zyss J. (Eds.), Nonlinear Optical Properties of Organic Molecules and Crystals, Vols. 1 and 2, Academic Press, NewYork. 1987.
8. Duan XL, Yuan DR, Wang XQ, Cheng XF, Yang ZH, Guo SY, Sun HQ, Xu D and Lu MK. Crys Res Tech. 2002;37:446-455.
9. Nalwa H and Seisomiyata (Eds.), Nonlinear Optics of Organic Molecules and Polymers, R.C. Press. 1997.
10. Purohit G and Joshi GC. Indian J Pure Appl Phys. 2003;41:922-927.
11. Caroline ML, Kumaresan S, Aravindan PG, Mohamed MP and Mani G. Acta Crystallogr E Crystallogr Commun. 2015;71:0661-2.
12. Gaussian, Revision A, Frisch MJ, Trucks GW, Schlegel HB, Scuseria GE, Robb MA, Cheeseman JR, Scalmani G, Barone V, Petersson GA, Nakatsuji H, Li X, Caricato M, Marenich A, Bloino J, Janesko BG, Gomperts R, Mennucci B, Hratchian HP, Ortiz JV, Izmaylov AF, Sonnenberg JL, Williams-Young D, Ding F, Lipparini F, Egidi F, Goings J, Peng B, Petrone A, Henderson T, Ranasinghe D, Zakrzewski VG, Gao J, Rega N, Zheng G, Liang W, Hada M, Ehara M, Toyota K, Fukuda R, Hasegawa J, Ishida M, Nakajima T, Honda Y, Kitao O, Nakai H, Vreven T, Throssell K, Montgomery JA, Jr Peralta JE, Ogliaro F, Bearpark M Heyd JJ, Brothers E, Kudin KN, Staroverov VN, Keith T, Kobayashi R, Normand J, Raghavachari K, Rendell A, Burant JC, Iyengar SS, Tomasi J,

Cossi M, Millam JM, Klene M, Adamo C, Cammi R, Ochterski JW, Martin RL, Morokuma K, Farkas O, Foresman JB and Fox DJ. Gaussian Inc. Wallingford CT. 2016.
13. Dennington RI, Keith T, Millam J, Eppinnett K and Hovell W. Gauss View, Version 3.09, 2003.
14. Anie Roshan S, Joseph C and Ittyachen MA. Matter Lett. 2001;49:299-302.
15. Venkataramanan V, Maheswaran S, Sherwood JN and Bhat HL. J Cryst Growth. 1997;173 (3-4):605-610.
16. Tigau N, Ciupinaa V, Prodana G, Rusub GI, Gheorghies C and Vasilec E. J Optoelectron Adv Mater. 2004;6:211-217.
17. Joshi VN. Photoconductivity: Art, Science and Technology, Marcel Dekker, New York. 1990.
18. Bamzai KK, Kotru PN and Wanklyn BM. Appl Surf Sci. 1998;133:195-204.
19. Onitsch EM. Microscopia.1947;2:131-151.
20. Hanneman M. Metall Manch. 1941;23:135-139.
21. Wooster WA. Rep Prog Phys. 1953;16:62-82.
22. Kurtz SK and Perry TT. J Appl Phys. 1968;39:3798-3813.
23. Glendening ED, Reed AE, Carpenter JE and Weinhold F. NBO Version 3.1, Theoretical Chemistry Institute and Department of Chemistry, University of Wisconsin.